ADVANCED FUNCTIONAL MATERIALS

FULL PAPER

DOI: 10.1002/adfm.200701526

Thermo-electrochemical Activation of an In–Cu Intermetallic Electrode for the Anode in Lithium Secondary Batteries**

By *Yoon S. Jung, Kyu T. Lee, Jun H. Kim, Ji Y. Kwon,* and *Seung M. Oh**

Lithium ion batteries (LIBs) have been emerging as a major power source for portable electronic devices and hybrid electric vehicles (HEV) with their superior performance to other competitors. The performance aspects of energy density and rate capability of LIBs should, however, be further improved for their new applications. Towards this end, many Li-alloy materials, metal oxides, and phosphides have been tested, some of which have, however, been discarded because of poor activity at ambient temperature. Here, it is shown that the In–Cu binary intermetallic compound (Cu_7In_3), which shows no activity at room temperature as a result of activation energy required for In–Cu bond cleavage, can be made active by discharge–charge cycling at elevated temperatures. Upon lithiation at elevated temperatures (55–120 °C), the Cu_7In_3 phase is converted into nanograins of metallic Cu and a lithiated In phase ($Li_{13}In_3$). The underlying activation mechanism is the formation of new In-rich phase (CuIn). The de-lithiation temperature turns out to be the most important variable that controlling the nature of the In-rich compounds.

1. Introduction

Li-alloy materials have been considered as an alternative anode to graphites since they have a high theoretical capacity ($Li_{15}Si_4$: 3579 mA h g^{-1}, $Li_{22}Sn_5$: 993 mA h g^{-1}, and graphite: 372 mA h g^{-1}).[1–6] They have not, however, been used as an anode in a practical battery mainly because of a severe volume change with cell cycling, which frequently leads to a disintegration of electrode materials and eventual capacity decay.[7,8] As an approach to overcome or at least alleviate this problem, active/inactive-type binary intermetallic compounds have been investigated: Cu_6Sn_5,[9,10] Fe_xSn,[11] Ni_xSn,[12] Co_xSn,[13,14] and $CoSb_3$.[15] These materials react with Li either by a simple addition-type reaction ($AB_x + yLi^+ + ye^- \rightarrow Li_yAB_x$) or conversion reaction ($AB_x + yLi^+ + ye^- \rightarrow Li_yA + xB$, A: active element and B: inactive element).[8,9,15] In the former reaction, Li^+ ions are simply inserted into the AB_x lattice along with electrons while the structural integrity is maintained. In the latter reaction, however, Li reacts with the active A component that is generated after A–B bond cleavage. The inactive component (B) supposedly plays a buffering role against the massive volume change encountered in the active component (A).[8–16]

The previous literature complains that many binary intermetallic compounds are inactive or show a much lower capacity than the theoretical one at room temperature, even if the reactions are thermodynamically feasible; Ni_xSn,[12] Co_3Sn_2,[14] Cu_3Si,[17] Ni_xSi,[18] Cu_3Sn,[19] and Al–M (M = Cr, Fe, Mn, and Ni) alloys.[20,21] Simply, such a slow kinetics can be attributed to a high activation energy needed either for Li^+ ion insertion (addition-type reaction) or for A–B bond cleavage (conversion reaction).[10,20,21] A more systematic study is, however, needed in order to address the kinetic barriers in these materials and to further find a way to enhance their reactivity, which is the major concern in this work. We studied the electrochemical reactivity and structural change upon lithiation of an In-containing binary intermetallic compound (Cu_7In_3), which is inactive for lithiation at room temperature. The major concern was the identification of reaction type (addition or conversion reaction) and the nature of the activation barriers that impede the lithiation reaction. Another output from this work, which should be highlighted, is the development of thermo-electrochemical activation.

2. Results and Discussion

2.1. Reaction Pathway and Kinetic Aspects of Cu_7In_3 Electrode

Figure 1 shows the galvanostatic discharge (lithiation, downward profiles) and charge (de-lithiation, upward) voltage profiles of pure In/Li and Cu_7In_3/Li cells at 25 and 120 °C. An immediately apparent feature here is that the Cu_7In_3 electrode

[*] Prof. S. M. Oh, Dr. Y. S. Jung,[+] Dr. K. T. Lee,[++] J. H. Kim
J. Y. Kwon
Department of Chemical and Biological Engineering and Research Centre for Energy Conversion and Storage
Seoul National University
Seoul, 151-744 (Korea)
E-mail: seungoh@snu.ac.kr

[+] Present address: Department of Mechanical Engineering, University of Colorado at Boulder, Boulder, CO 80309-0427 (USA)

[++] Present address: Department of Chemistry
University of Waterloo Ontario, N2 L3G1 (Canada)

[**] This work was supported by KOSEF through the Research Centre for Energy Conversion and Storage. Supporting Information is available online from Wiley InterScience or from the author.

ADVANCED FUNCTIONAL MATERIALS

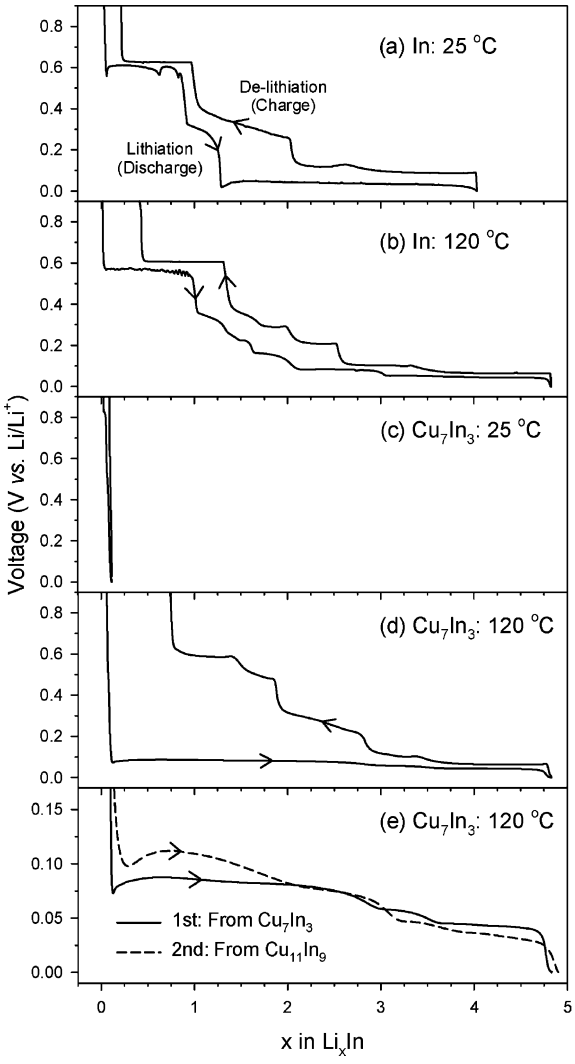

Figure 1. a–d) Galvanostatic discharge–charge voltage profiles of pure In/Li and Cu_7In_3/Li cells. e) The enlarged view of discharge voltage profiles of Cu_7In_3 electrode. The second profile corresponds to that of $Cu_{11}In_9$ since this phase is generated after a cycling. Specific current was 10 mA g_{In}^{-1} (~0.01 C-rate) at 25 °C and 100 mA g_{In}^{-1} at 120 °C.

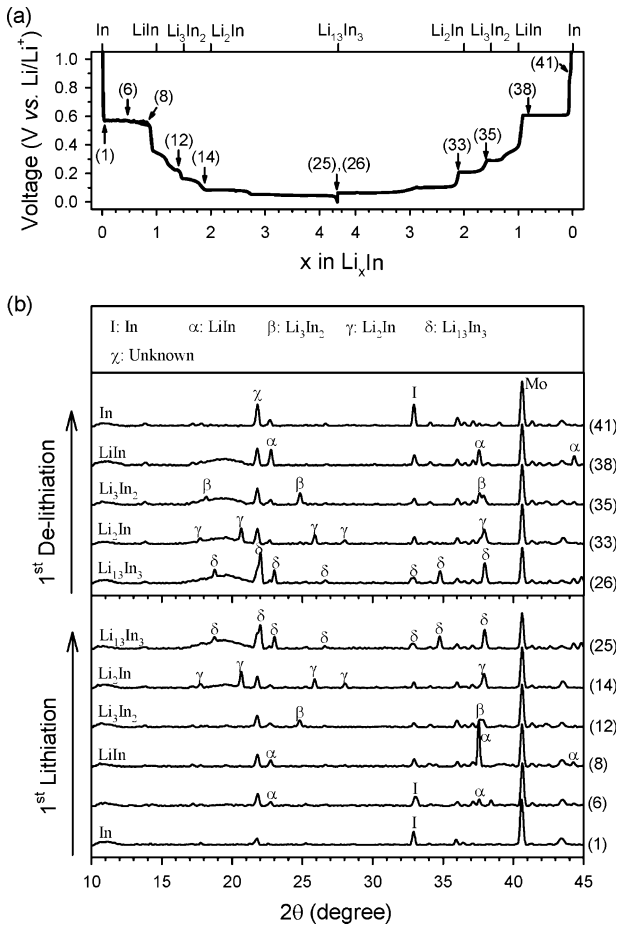

Figure 2. a) Discharge–charge voltage profile of pure In/Li cell obtained at 120 °C. The capacity was normalized by the value of $Li_{13}In_3$ (theoretical specific capacity = 1012 mA h g^{-1}). The phases evolved during lithiation/de-lithiation are indicated at the top. b) In-situ XRD patterns of pure In electrode that were obtained with a 50 mA h g_{In}^{-1} interval. The numbers in parenthesis indicate the scan number. An unknown phase denoted as 'χ' likely comes from an irreversible decomposition product since it steadily grows with time.

is inactive for lithiation at 25 °C under the current cycling condition (Fig. 1c), but becomes active at 120 °C (Fig. 1d). The pure In electrode, however, shows a reversible discharge–charge behavior at both temperatures with several voltage plateaus, which reflects that many Li-containing In phases (Li_xIn) are involved in the lithiation/de-lithiation process (Figs. 1a and 1b). One curious feature is that even if the Cu_7In_3 electrode is active at 120 °C, its voltage profile is somewhat different to that of pure In. The most noticeable difference is the single voltage plateau that appears in the earlier period of lithiation from $x = 0.0$ to 2.0 for Li_xIn (from Cu_7In_3 to Li_2In) (Fig. 1d), which is contrasted by at least three plateaus in the pure In electrode (Fig. 1b).

The in-situ X-ray diffraction (XRD) patterns that were obtained during the first lithiation/de-lithiation period at 120 °C are displayed in Figure 2 (pure In) and Figure 3 (Cu_7In_3 electrode). The lithiated In phases have been identified by XRD analysis on the coexisting phases in the plateau regions. For instance, a careful inspection of the XRD data taken at the first plateau region (0.56 V in Fig. 2a) reveals that only a metallic In phase appears (at 33°) in the first scan (Fig. 2b). In the sixth scan, however, the LiIn phase (indicated by α) develops at the expense of the In phase, which must be a result of lithiation. The LiIn phase becomes dominant over In at the eighth scan. This explains that In is present as the metallic state before this plateau, whereas it is present in the LiIn phase at the end of plateau. A similar phase analysis was made on all the plateaus (four plateaus in lithiation and four plateaus in de-lithiation), from which we can identify the lithiated In (Li_xIn) phases that are evolved in the course of cycling (top of Fig. 2a). These phases are well matched with what are predicted from the lithiation/de-lithiation capacity within experimental error

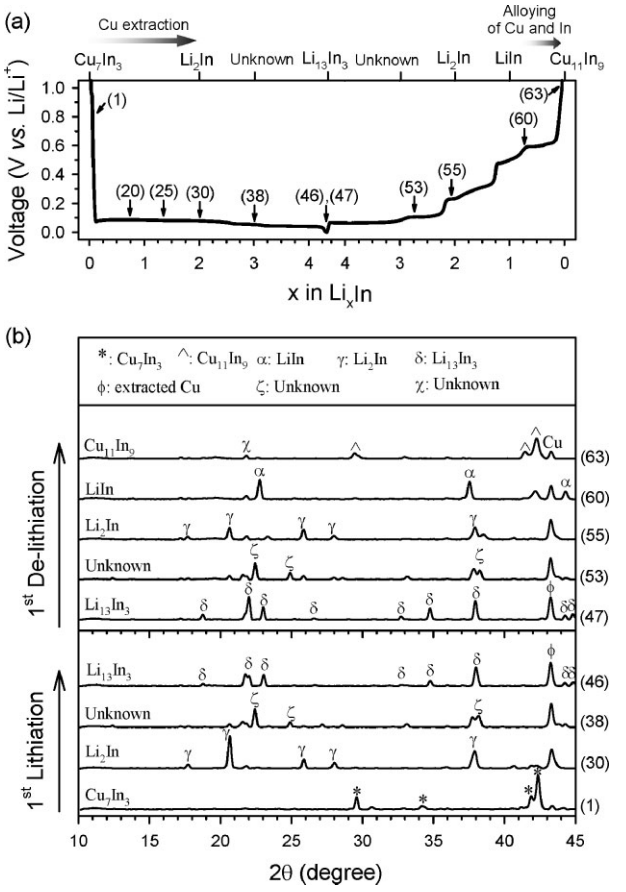

Figure 3. a) Discharge–charge voltage profile of Cu_7In_3/Li cell obtained at 120 °C. The capacity was normalized by the value of $Li_{13}In_3$ (theoretical specific capacity = 1012 mA h g_{In}^{-1}). The phases evolved during lithiation/de-lithiation are indicated at the top. b) In-situ XRD patterns that were obtained with a 50 mA h g_{In}^{-1} interval. The numbers in parenthesis indicate the scan number. An unknown phase (ζ) seems to be one of the lithiated In phases, but could not be indexed.

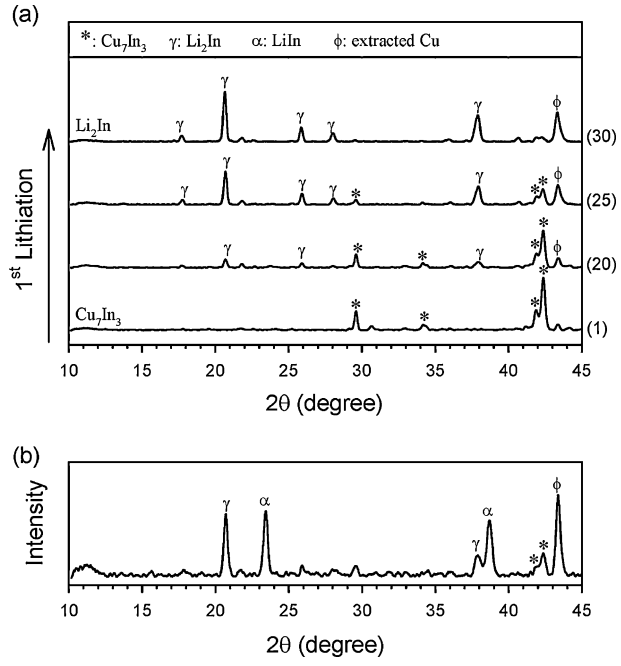

Figure 4. a) In-situ XRD patterns of a Cu_7In_3 electrode for the initial 30 scans (Fig. 3). Note that the initial Cu_7In_3 phase (*) is converted into Li_2In (γ) and metallic Cu (ϕ) in this range. b) Ex-situ XRD pattern of a Cu_7In_3 electrode lithiated to LiIn at 120 °C. The electrode was lithiated with a specific current of 30 mA g_{In}^{-1} for 10 h at 120 °C and transferred to the XRD cell, the temperature of which was kept at 120 °C for 3 h before the measurement.

(bottom scale in Fig. 2a). The following reversible lithiation/de-lithiation pathway is identified for the pure In electrode:

$$In \leftrightarrow LiIn \leftrightarrow Li_3In_2 \leftrightarrow Li_2In \leftrightarrow Li_{13}In_3$$

The phases were indexed as follows; In (JCPDS no. 00-005-0642), LiIn (JCPDS no. 03-065-5507), Li_3In_2 (JCPDS no. 00-033-0616), Li_2In (JCPDS no. 00-033-0614), $Li_{13}In_3$ (JCPDS no. 00-033-0615), Cu_7In_3 (JCPDS no. 03-065-2249), and $Cu_{11}In_9$ (JCPDS no. 03-065-4963). In short, the pure In electrode is lithiated with up to 4.3 Li atoms ($Li_{13}In_3$, theoretical specific capacity = 1012 mA h g^{-1}) and fully recovered to metallic In after de-lithiation.

The reaction pathway of the Cu_7In_3 electrode at 120 °C is similar to that of pure In as it is also fully lithiated to a $Li_{13}In_3$ phase (Figs. 1d and 3a), but differs in many aspects. First of all, Cu atoms are extracted at the earlier period of lithiation from $x = 0.0$ to 2.0 for Li_xIn (from Cu_7In_3 to Li_2In). For clarity, the XRD data taken in this region is separately presented in Figure 4a. Only the diffraction peaks that belong to the initial Cu_7In_3 are detected in the first scan. At the 20th scan, however, the Li_2In phase and extracted metallic Cu (43°) develop at the expense of Cu_7In_3, which reflects that the initial Cu_7In_3 phase is converted into Li_2In and metallic Cu through Cu–In bond cleavage. That is, the Cu_7In_3 electrode is lithiated by a conversion reaction. At the 30th scan, only the diffraction peaks that belong to Li_2In and metallic Cu appear without any from Cu_7In_3, which suggests that the Cu–In bond cleavage is complete at this point. The absence of Li–In–Cu ternary phases in this region further supports that the Cu_7In_3 is not lithiated by an addition-type reaction but directly by a conversion reaction.[10,20,21] Another difference between the two electrodes is that Cu_7In_3 is lithiated directly to Li_2In in this region (Fig. 4a), but via the intermediate phases (LiIn and Li_3In_2) in the pure In electrode. In order to see if this behavior has a kinetic or thermodynamic origin, XRD measurements were performed after the Cu_7In_3 electrode was lithiated up to approx. one Li per In (LiIn phase) and rested for 3 h at 120 °C. As seen in Figure 4b, the LiIn phase is detected, which indicates that the absence of intermediate phases (LiIn and Li_3In_2) is not a result of thermodynamics, but has a kinetic origin. That is, the formation of two intermediate phases is thermodynamically allowed, but has been missed since the specific current (30 mA g_{In}^{-1}) used in this experiment was too large. If the sweeping rate is extremely low, the phases seem to appear.

ADVANCED FUNCTIONAL MATERIALS

A comparison of the voltage profiles (Figs. 2a and 3a) illustrates that the lithiation voltage of the Cu_7In_3 electrode in the Cu extraction region is much lower than that for the pure In electrode. To account for this, both thermodynamic and kinetic considerations should be made. With respect to the thermodynamics, the equilibrium potential for lithiation should differ between the two since the free energy of formation (ΔG_f°) should be considered as indicated in Equation (1).

$$E_2^{\circ} = E_1^{\circ} + \frac{\Delta G_f^{\circ}(AB_x)}{nF} \quad (1)$$

Here, E_1° and E_2° are the lithiation equilibrium potentials for a pure In and a Cu_7In_3 electrode, respectively. These values were obtained by measuring the rest potentials (Fig. 5). The equilibrium (rest) potential (E_1°) at the nominal composition of $Li_{0.5}In$, which lies within the first plateau region in Figure 2a, is 0.60 V (vs. Li/Li^+). The marginal difference between this and the transient voltage suggests a negligible overpotential under this current condition (100 mA g_{In}^{-1}). The E_2° value is 0.41 V, which is lower by as much as 0.19 V as compared with the pure In electrode. An appreciable amount of overpotential (0.31 V) is also observed in this electrode. From this, the lower lithiation voltage observed with the Cu_7In_3 electrode in the single plateau region (Fig. 3a) can be accounted for partially by the lower lithiation potential (thermodynamic consideration) and larger overpotential (kinetic aspect) as compared with those for the pure In electrode. Furthermore, the large overpotential encountered in the Cu_7In_3 electrode can be related to the activation energy needed for In–Cu bond cleavage since the bond cleavage does occur in the same composition range (from Cu_7In_3 to Li_2In) (XRD data in Fig. 4a). The poor lithiation activity at room temperature for this electrode (Fig. 4c) can also be accounted for by this activation energy.

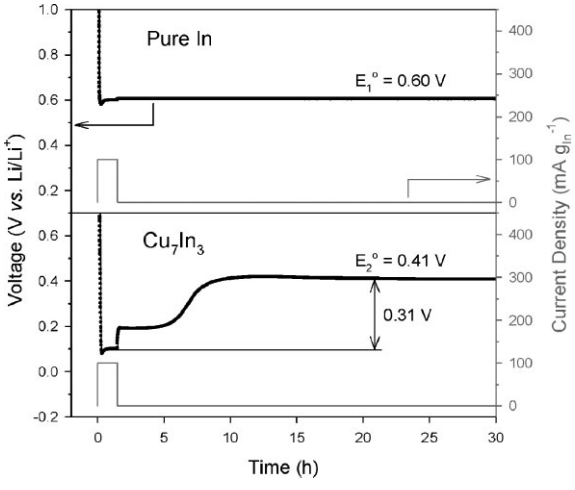

Figure 5. The voltage profiles for lithiation and open-circuit condition for a) a pure In/Li and b) a Cu_7In_3/Li cell. Both electrodes were lithiated up to $x = 0.5$ for Li_xIn at 120 °C at a current density of 100 mA g_{In}^{-1} and rested under open-circuit conditions to measure the equilibrium potential for the first lithiation step.

The de-lithiation pathway of the Cu_7In_3 electrode also differs to that for pure In. The XRD data reveals that an unknown phase (ζ) is evolved between Li_2In and $Li_{13}In_3$, and the Li_3In_2 phase is missing (Figs. 2b and 3b). This feature can also be explained by taking account of kinetic and thermodynamic considerations. An example that illustrates that the absence of intermediate phases is caused by kinetic origins has already been given above. An unusual alteration of thermodynamics has also been reported in many nanosized composite materials, where the surface-to-volume ratio is so large that the surface energy is a more dominant factor than the internal energy in controlling the thermodynamics of the system.[15,22–32] In this work, in order to see if the extracted Cu and Li_xIn phases are indeed present as a nanosized composite, annular dark field-scanning transmission electron microscopy (ADF-STEM) was performed and energy dispersive spectroscopy (EDS) elemental maps were taken for the Cu_7In_3 electrode. As seen in Figure 6, the nanosized (<50 nm) Cu and LiIn phase are evenly distributed over the electrode layer. Their particle size was calculated using the Scherrer equation with the XRD data (Fig. 3b) to be 20–40 nm. Hence, the unusual thermodynamic properties observed in this work, the presence of unexpected phases, and absence of intermediate phases, can now be explained by taking account of the importance of surface energy claimed in many nanosystems. The difference in the reaction pathways (evolution of intermediate Li_xIn phases) between the two electrodes is difficult to understand since metallic In is generated after Cu–In bond cleavage (conversion reaction). That is, the as-generated In phase should exhibit the same thermodynamic behaviour (phase evolution) as pure In because the two are the same metallic In. One important difference between the two, however, is the presence of nanosized metallic Cu in the Cu_7In_3 electrode. Hence, one can assume that the thermodynamic properties of metallic In that is generated from the Cu_7In_3 phase are affected by the co-existing metallic Cu. This assumption, however, seems to be valid only if the metallic Cu and In are in intimate contact with each other with a large surface area, which is the case in this work as shown in Figure 6. A similar observation was made by us with another intermetallic electrode ($CuGa_2$), wherein some lithiated phases are missing and unexpected phases are evolved with cycling.[32] This unusual thermodynamic behaviour has been explained by the alteration of surface energy of Li_xGa nanograins, which is caused by partial bonding between two components. The presence of partial bonding between Cu and Ga atoms of the Li_xGa phases has been evidenced by Raman spectroscopy.

2.2. Thermo-electrochemical Activation of a Cu_7In_3 Electrode

The reaction pathway shown in Figure 3a illustrates that metallic Cu, which is extracted in the bond cleavage region, remains in a metallic state but recombines with metallic In that

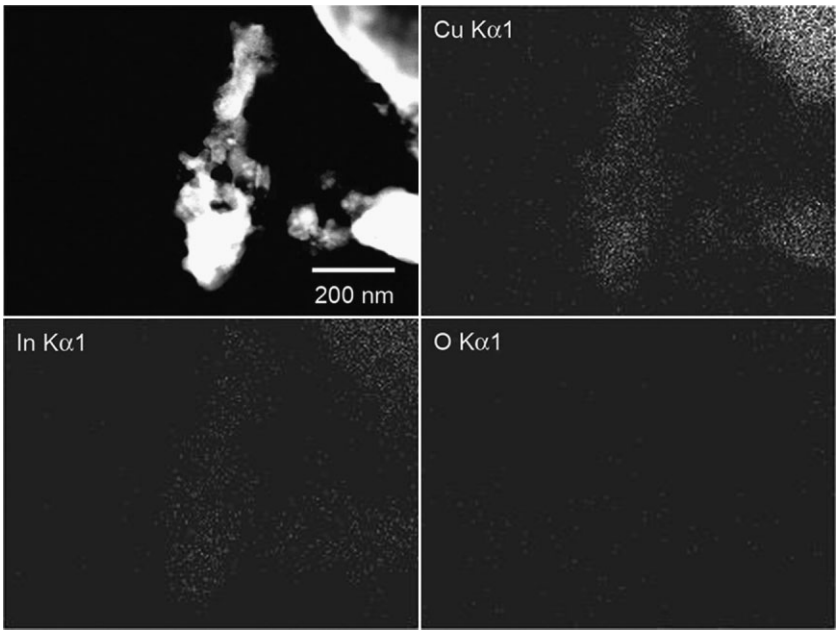

Figure 6. ADF-STEM image and element maps for LiIn and Cu phases obtained from a Cu_7In_3 electrode. The element map shows the local EDS signal of Cu, In, and O, respectively. Oxidation of LiIn can be ignored from the negligible intensity of O. The Cu_7In_3 electrode was lithiated to 0.0 V (vs. Li/Li^+) and de-lithiated to 0.4 V with 50 mA g_{In}^{-1} at 55 °C to generate LiIn phase.

is restored at the final stage of de-lithiation. However, the final product after a cycle is not the initial Cu_7In_3 but the $Cu_{11}In_9$ phase. Note that the Cu content in this new phase is smaller than that in the Cu_7In_3 phase, which indicates that all the extracted Cu is not recombined with metallic In. The lithiation activity is compared for two phases in Figure 1e, where the first lithiation profile is for the Cu_7In_3 phase whereas the second one is for the new phase ($Cu_{11}In_9$). A valuable piece of information gained from Figure 1e is that the In-rich (inversely, Cu-deficient) phase exhibits a higher lithiation voltage in the Cu–In bond cleavage region, manifesting itself that the new phase is more active for lithiation. It is a common observation that A-rich A–B intermetallics are more reactive for lithiation,[11,13,14,33] which is also the case for the In–Ni binary intermetallics as shown in the Supporting Information: The In-rich compounds show a higher lithiation activity; $Ni_2In_3 > Ni_3In$. This feature can be rationalized by both thermodynamic and kinetic considerations. From a thermodynamic point of view, A-rich A–B intermetallics should show a more positive lithiation equilibrium potential because they have a less negative free energy of formation per one mole of AB_x (refer to Equation (1)).[34] From a kinetic consideration, A-rich A–B intermetallics should have a higher reactivity because they have a smaller number of A–B bonds to be broken.

From the observation whereby the In-rich compound ($Cu_{11}In_9$) shows a higher lithiation activity than the initial one (Cu_7In_3), we assumed that the room-temperature inactive Cu_7In_3 phase can be converted into active ones if it is converted into more In-rich phases. To generate In-rich compounds, the working temperature was varied in this work. Figure 7 presents the ex-situ XRD patterns of Cu_7In_3 electrodes that were cycled with a variation in the temperatures. The top three XRD patterns were obtained by varying the de-lithiation temperature while the lithiation temperature was fixed at 85 °C. The sample de-lithiated at 85 °C gives rise to the diffraction peaks that belong to the $Cu_{11}In_9$ phase. Upon de-lithiation at 25 °C, however, the recovered phase turns out to be CuIn (JCPDS no. 00-035-1150). The generation of a mixture of $Cu_{11}In_9$ and CuIn by a de-lithiation at 55 °C suggests that more In-rich compounds are generated with a decrease in the de-lithiation temperature. The room-temperature lithiation activity is compared for these new phases (Fig. 8), where the generated phases and lithiation/de-lithiation temperature are indicated in the inset. Note that the cycling condition for the three samples is the same as for Figures 7a–7c. The sample that was de-lithiated at 85 °C (Fig. 8a) exhibits a negligible activity for lithiation, which means that the $Cu_{11}In_9$ phase is also inactive at room temperature. The sample de-lithiated at 25 °C (CuIn), however, shows a much higher activity with a discharge capacity that approaches the theoretical value ($Li_{13}In_3$, 1012 mA h g^{-1}) at room temperature. The sample de-lithiated at 55 °C that is a mixture of $Cu_{11}In_9$ and CuIn shows an intermediate behavior. When the lithiation activity is compared for Cu_7In_3 (Fig. 1c) and CuIn (Fig. 8c) at 25 °C, one can recognize a superior activity in the latter. We named this phenomenon 'thermo-electrochemical activation' since the inactive phase (Cu_7In_3) is converted into an active one (CuIn) by an electrochemical reaction at elevated temperatures.

The XRD patterns in Figures 7d–7f give an insight into the underlying activation mechanism. For Figure 7d, the Cu_7In_3 electrode was lithiated only up to 2.5 Li per one In atom ($Li_{2.5}In$), which is just beyond the Cu extraction region (Li_2In), and de-lithiated at 25 °C. As shown, the recovered phase is CuIn, the same one that was obtained after a full lithiation to $Li_{13}In_3$ (Fig. 7c). This suggests that the prerequisite for thermo-electrochemical activation is the Cu–In bond cleavage. That is, the activation is allowed if the lithiation is extended beyond the Cu extraction region. Figures 7e and 7f eloquently demonstrate the importance of de-lithiation temperature in the activation process. The samples were lithiated at 55 °C, which is lower than that (85 °C) for Figure 7b and 7c, and de-lithiated at two different temperatures. The CuIn phase is generated after de-lithiation at 25 °C but the mixture is generated at 55 °C, which indicates that the same product is formed if the de-lithiation temperature is the same. This feature is not difficult to

ADVANCED FUNCTIONAL MATERIALS

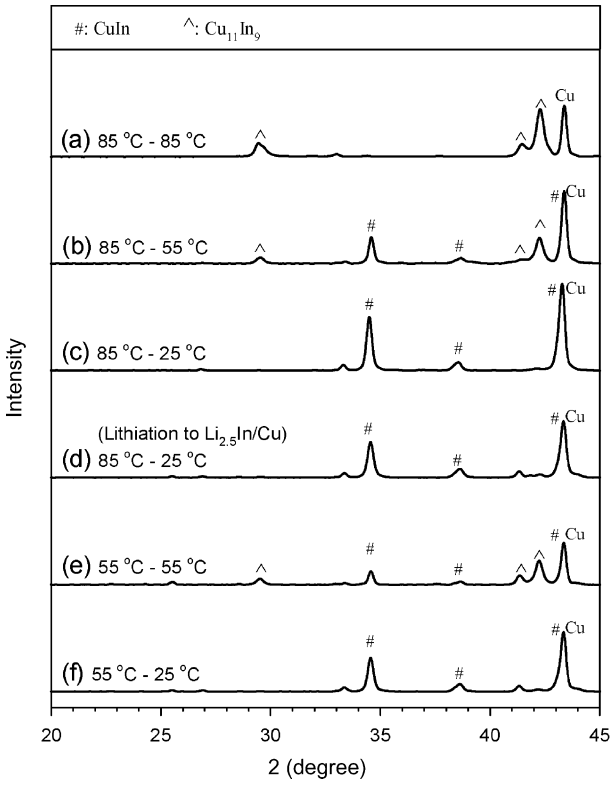

Figure 7. Ex-situ XRD results obtained after thermo-electrochemical activation of Cu_7In_3 electrodes. The electrodes were lithiated and de-lithiated in the range of 0.0–2.0 V (vs. Li/Li^+). Specific current was 100 mA g_{In}^{-1} except for lithiation at 55 °C (20 mA g_{In}^{-1}). The lithiation and de-lithiation temperature are given in the inset. For d), the electrode was lithiated to a nominal composition of $Li_{2.5}In$ (capacity = 584 mA h g_{In}^{-1}) and de-lithiated.

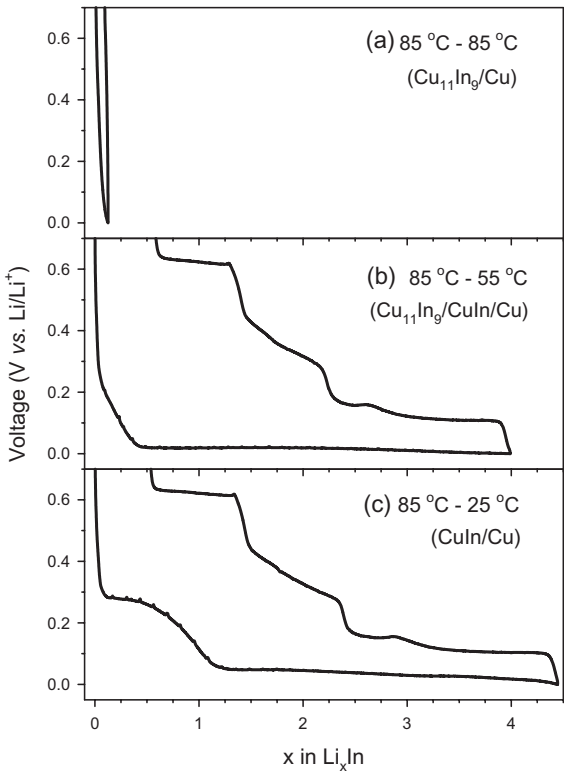

Figure 8. Room-temperature (25 °C) discharge–charge voltage profiles obtained after thermo-electrochemical activation of Cu_7In_3/Li cells. The specific current was 10 mA g_{In}^{-1}. The generated In-rich phases are indicated in the inset. The lithiation and de-lithiation temperature for activation (provided in the inset) was the same as for Figures 7a–7c

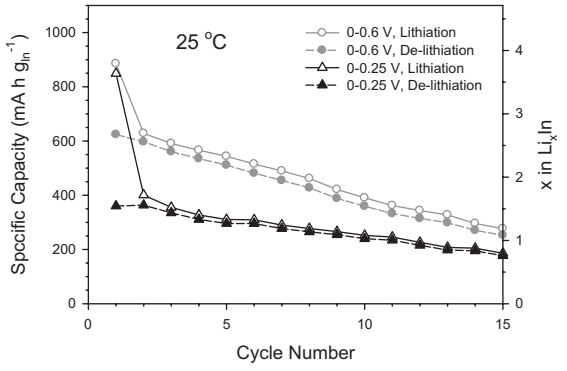

Figure 9. Room-temperature cycle performance of an CuIn phase that was generated by thermo-electrochemical activation of a Cu_7In_3 electrode; lithiation at 85 °C and de-lithiation at 25 °C. The specific current was 30 mA g_{In}^{-1} at 25 °C.

understand since the new phase formation takes place at the end of the de-lithiation period.

Figure 9 provides the room-temperature cycle performance of a CuIn phase that was generated by thermo-electrochemical activation; lithiated at 85 °C and de-lithiated at 25 °C. The cycle performance is not highly promising since the capacity steadily decreases. This unsatisfactory observation has seemingly come from the intrinsic property of In, rather than any problems encountered with activation. That is, one can readily expect a severe volume expansion/contraction during the alloying/de-alloying of the In component that is generated after the bond cleavage. The thermo-electrochemical activation may be extended to other systems since there are many intermetallic compounds, metal oxides, phosphides, and nitrides that have been discarded as a result of poor activity at ambient temperature.[17–21,35] From a practical point of view, thermo-electrochemical activation can be employed in a practical cell manufacturing process since the elevated-temperature formation process, the pre-charge–discharge cycling of commercial cells before they come into the market, is commonly adopted.[36,37] The thermo-electrochemical activation can be carried out at this formation period.

3. Conclusions

In this paper, we demonstrate a way to activate room-temperature inactive electrode materials by a discharge–charge cycling at elevated temperatures. The results are summarized in the following two points.

1) The Cu_7In_3 electrode is inactive at room temperature under a normal discharge–charge cycling condition. The

in-situ XRD study made at 120 °C illustrates that the lithiation proceeds by a conversion reaction, wherein metallic Cu and In are separated by a bond cleavage during the earlier lithiation period ($x = 0.0$–2.0 for Li_xIn). The galvanostatic discharge–charge voltage profile shows that the electrode polarization is most serious in the bond cleavage region, which can be ascribed to a lower equilibrium potential for lithiation (thermodynamic consideration) and larger overpotential (kinetic aspect) as compared with those for the pure In electrode. The latter feature is deeply associated with the activation energy required for In–Cu bond cleavage. The extracted Cu remains as a metallic state until it chemically recombines with metallic In that is generated at the final stage of de-lithiation. An In-rich compound ($Cu_{11}In_9$) was generated at 120 °C, which is more reactive than the Cu_7In_3 phase.

2) The Cu_7In_3 phase was activated by discharge–charge cycling at elevated temperatures. The as-generated In-rich phase (CuIn) can be discharged to the $Li_{13}In_3$ phase at room temperature. The formation of this phase is favored by lowering the de-lithiation temperature in the activation process. The prerequisite for activation turns out to be the formation of nanosized metallic Cu and lithiated In phases by Cu–In bond cleavage.

4. Experimental

For the electrochemical characterization, the pure In and Cu_7In_3 electrodes were prepared as a thick film (thickness ~4 μm) by using a DC sputtering method (power density = 1.2 kW, base pressure = 1.0×10^{-5} torr, and working pressure = 5 mtorr with Ar). For the pure In electrode, a thick film of In was deposited on Mo foil (25 μm) since alloy formation between In and Mo is negligible. For the Cu_7In_3 electrode, however, an In film was deposited on a piece of Cu foil (25 μm) and then heat-treated at 285 °C for 6 days under vacuum. For the in-situ XRD analysis, the foil current collector was replaced by Mo and Cu mesh because, with the foil current collector, the electrode layer was not easily accessed by the electrolyte solution because of a very narrow gap between the electrode and beryllium window in the electrochemical XRD cell. With the meshes, however, the electrolyte solution could easily penetrate into the electrode layer through the holes.

For the ADF-STEM and EDS elemental mapping, the electrode samples were prepared as a powder form and formulated as a composite electrode by using Cu foil as the current collector. The Cu_7In_3 powder was prepared by heating a stoichiometric mixture of Cu and In powder at 285 °C for 6 days under vacuum, which was followed by high-energy ball-milling for 3 h and heat-treatment at 285 °C under vacuum for 6 days. The composite electrode was prepared by spreading a slurry mixture of Cu_7In_3 powder, Super P (as a carbon additive for conductivity enhancement), and PVDF (poly(vinylidene fluoride), as a binder) (70: 15: 15, weight ratio) on a piece of Cu foil. All the chemicals were purchased from Aldrich and Alfa Aesar.

For the in-situ XRD analysis at elevated temperatures, a specially designed electrochemical cell with a beryllium window was mounted on a D8-Bruker diffractometer equipped with Cu Kα radiation (1.54056 Å). For the ex-situ XRD analysis, cells were disassembled and electrodes were rinsed with dimethyl carbonate and dried in an Ar-filled dry box. All the XRD patterns were recorded at 3 kV and 30 mA using a continuous scanning mode with 0.50 deg min^{-1}.

Two-electrode 2032-type coin cells were employed to assess the electrochemical characteristics. The cells were assembled in an Ar-filled dry box and tested in a temperature-controlled oven. The galvanostatic discharge–charge cycling was performed in the potential range of 0.0–2.0 V (vs. Li/Li^+). Li foils (Cyprous Co.) were used as the counter and reference electrode. 1.0 M lithium bis(oxalate)borate (LiBOB) in γ-butyrolactone (GBL) was used as the electrolyte. As the separator, a glass fiber sheet was used. Note that the specific capacity and current are expressed on the basis of weight of In component. In this report, lithiation was expressed as discharging but de-lithiation as charging because Li foil was used as the counter electrode in the half-cells.

Received: December 28, 2007
Revised: May 9, 2008
Published online: September 22, 2008

[1] Y. Idota, T. Kubota, A. Matsufuji, Y. Maekawa, T. Miyasaka, *Science* **1997**, *276*, 1395.
[2] M. Winter, J. O. Besenhard, M. E. Spahr, P. Novák, *Adv. Mater.* **1998**, *10*, 725.
[3] M. N. Obrovac, L. Christensen, *Electrochem. Solid-State Lett.* **2004**, *7*, A93.
[4] T. D. Hatchard, J. R. Dahn, *J. Electrochem. Soc.* **2004**, *151*, A838.
[5] D. Larcher, S. Beattie, M. Morcrette, K. Edström, J. C. Jumas, J.-M. Tarascon, *J. Mater. Chem.* **2007**, *17*, 3759.
[6] K. T. Lee, Y. S. Jung, S. M. Oh, *J. Am. Chem. Soc.* **2003**, *125*, 5652.
[7] L. Y. Beaulieu, K. W. Eberman, R. L. Turner, L. J. Krause, J. R. Dahn, *Electrochem. Solid-State Lett.* **2001**, *4*, A137.
[8] M. N. Obrovac, L. Christensen, D. B. Le, J. R. Dahn, *J. Electrochem. Soc.* **2007**, *154*, A849.
[9] K. D. Kepler, J. T. Vaughey, M. M. Thackeray, *Electrochem. Solid-State Lett.* **1999**, *2*, 307.
[10] D. Larcher, L. Y. Beaulieu, D. D. MacNeil, J. R. Dahn, *J. Electrochem. Soc.* **2000**, *147*, 1658.
[11] O. Mao, J. R. Dahn, *J. Electrochem. Soc.* **1999**, *146*, 414.
[12] H. Mukaibo, T. Sumi, T. Yokoshima, T. Momma, T. Osaka, *Electrochem. Solid-State Lett.* **2003**, *6*, A218.
[13] J. R. Dahn, R. E. Mar, A. Abouzeid, *J. Electrochem. Soc.* **2006**, *153*, A361.
[14] J. J. Zhang, Y. Y. Xia, *J. Electrochem. Soc.* **2006**, *153*, A1466.
[15] J.-M. Tarascon, M. Morcrette, L. Dupont, Y. Chabre, C. Payen, D. Larcher, V. Pralong, *J. Electrochem. Soc.* **2003**, *150*, A732.
[16] H. Inoue, Abstract #228, in International Meeting on Lithium Batteries (IMLB 2006), Biarritz, France, June 18–23, **2006**.
[17] J. H. Kim, H. Kim, H. J. Sohn, *Electrochem. Commun.* **2005**, *7*, 557.
[18] M. S. Park, Y. J. Lee, S. Rajendran, M. S. Song, H. S. Kim, J. Y. Lee, *Electrochim. Acta* **2005**, *50*, 5561.
[19] Y. Xia, T. Sakai, T. Fujieda, M. Wada, H. Yoshinaga, *J. Electrochem. Soc.* **2001**, *148*, A471.
[20] D. Larcher, L. Y. Beaulieu, O. Mao, A. E. George, J. R. Dahn, *J. Electrochem. Soc.* **2000**, *147*, 1703.
[21] M. D. Fleischauer, M. N. Obrovac, J. D. McGraw, R. A. Dunlap, J. M. Topple, J. R. Dahn, *J. Electrochem. Soc.* **2006**, *153*, A484.
[22] J. Jamnik, J. Maier, *Phys. Chem. Chem. Phys.* **2003**, *5*, 5215.
[23] Y. S. Hu, L. Kienle, Y. G. Gou, J. Maier, *Adv. Mater.* **2006**, *18*, 1421.
[24] M. Okubo, E. Hosono, J. Kim, M. Enomoto, N. Kojima, T. Kudo, H. Zhou, I. Honma, *J. Am. Chem. Soc.* **2007**, *129*, 7444.

ADVANCED FUNCTIONAL MATERIALS

[25] M. Wagemaker, W. J. H. Borghols, F. M. Mulder, *J. Am. Chem. Soc.* **2007**, *129*, 4323.
[26] K. Murakoshi, H. Hosokawa, N. Tanaka, M. Saito, Y. Wada, T. Sakata, H. Mori, S. Yanagida, *Chem. Commun.* **1998**, 321.
[27] N. Meethong, H. Y. S. Huang, W. C. Carter, Y. M. Chiang, *Electrochem. Solid-State Lett.* **2007**, *10*, A134.
[28] L. Kavan, M. Kalbác, M. Zukalová, I. Exnar, V. Lorezen, R. Nesper, M. Graetzel, *Chem. Mater.* **2004**, *16*, 477.
[29] L. Kavan, J. Procházka, T. M. Spitler, M. Kalbáč M. Zukalová, T. Drezen, M. Grätzel, *J. Electrochem. Soc.* **2003**, *150*, A1000.
[30] G. Sudant, E. Baudrin, D. Larcher, J.-M. Tarascon, *J. Mater. Chem.* **2005**, *15*, 1263.
[31] J. Maier, *Nat. Mater.* **2005**, *4*, 805.
[32] K. T. Lee, Y. S. Jung, J. Y. Kwon, J. H. Kim, S. M. Oh, *Chem. Mater.* **2008**, *20*, 447.
[33] A. D. W. Todd, R. E. Mar, J. R. Dahn, *J. Electrochem. Soc.* **2006**, *153*, A1998.
[34] F. R. de Boer, R. Boom, W. C. M. Mattens, A. R. Miedema, A. K. Niessen, in *Cohesion in Metals Transition Metal Alloys*, Vol. 1(Eds: F. R. de Boer, D. G. Pettifor), Elsevier Science, Amsterdam, The Netherlands **1988**, Ch.3.
[35] H. Li, P. Balaya, J. Maier, *J. Electrochem. Soc.* **2004**, *151*, A1878.
[36] S. Zhang, M. S. Ding, K. Xu, J. Allen, T. R. Jow, *Electrochem. Solid-State Lett.* **2001**, *4*, A206.
[37] P. C. J. Chiang, M. S. Wu, J. C. Lin, *Electrochem. Solid-State Lett.* **2005**, *8*, A423.